













RESEARCH ARTICLE

Innovative Tools and Methods

Lipid fingerprint-based histology accurately classifies nevus, primary melanoma, and metastatic melanoma samples

Cristina Huergo-Baños¹  | Verónica Velasco^{2,3}  | Jone Garate¹  |
 Roberto Fernández¹ | Javier Martín-Allende⁴  | Ignacio Zabalza^{3,5} |
 Juan L. Artola^{3,6} | Rosa M. Martí^{7,8}  | Aintzane Asumendi^{3,9}  |
 Egoitz Astigarraga¹⁰  | Gabriel Barreda-Gómez¹⁰  | Olatz Fresnedo¹¹  |
 Begoña Ochoa¹¹  | María D. Boyano^{3,9}  | José A. Fernández¹ 

¹Department of Physical Chemistry, Faculty of Science and Technology, University of the Basque Country (UPV/EHU), Leioa, Spain

²Department of Pathology, Cruces University Hospital, Barakaldo, Spain

³Biocruces-Bizkaia Health Research Institute, Cruces University Hospital, Barakaldo, Spain

⁴Languages and Computer Systems, School of Engineering University of the Basque Country (UPV/EHU), Bilbao, Spain

⁵Department of Pathology, Galdakao-Usansolo University Hospital, Galdakao, Spain

⁶Department of Dermatology, Galdakao-Usansolo University Hospital, Galdakao, Spain

⁷Department of Dermatology, Arnau de Vilanova University Hospital, Institute of Biomedic Research (IRBLleida), University of Lleida, Lleida, Spain

⁸Centre of Biomedical Research on Cancer (CIBERONC), Instituto de Salud Carlos III (ISCIII), Madrid, Spain

⁹Department of Cell Biology and Histology, Faculty of Medicine and Nursing, University of the Basque Country (UPV/EHU), Leioa, Spain

¹⁰Department R+D, IMG Pharma Biotech S.L., Derio, Spain

¹¹Department of Physiology, Faculty of Medicine and Nursing, University of the Basque Country (UPV/EHU), Leioa, Spain

Correspondence

María D. Boyano, Department of Cell Biology and Histology, Faculty of Medicine and Nursing, University of the Basque Country (UPV/EHU), Barrio Sarriena, s/n, 48940 Leioa, Spain.

Email: lola.boyano@ehu.es

José A. Fernández, Department of Physical Chemistry, Faculty of Science and Technology, University of the Basque Country (UPV/EHU), Barrio Sarriena, s/n, 48940 Leioa, Spain.

Email: josea.fernandez@ehu.es

Funding information

Agencia Estatal de Investigación, Grant/Award Number: RTC-2015-3693-1; Basque Government, Grant/Award Numbers: IT1491-22, KK2017-041, KK2020-00069; Euskal Herriko Unibertsitatea, Grant/Award Number: GIU17/066

Abstract

Probably, the most important factor for the survival of a melanoma patient is early detection and precise diagnosis. Although in most cases these tasks are readily carried out by pathologists and dermatologists, there are still difficult cases in which no consensus among experts is achieved. To deal with such cases, new methodologies are required. Following this motivation, we explore here the use of lipid imaging mass spectrometry as a complementary tool for the aid in the diagnosis. Thus, 53 samples (15 nevus, 24 primary melanomas, and 14 metastasis) were explored with the aid of a mass spectrometer, using negative polarity. The rich lipid fingerprint obtained from the samples allowed us to set up an artificial intelligence-based classification model that achieved 100% of specificity and precision both in training and validation data sets. A deeper analysis of the image data shows that the technique reports important information on the tumor microenvironment that may give invaluable insights in the prognosis of the lesion, with the correct interpretation.

This is an open access article under the terms of the [Creative Commons Attribution-NonCommercial](https://creativecommons.org/licenses/by-nc/4.0/) License, which permits use, distribution and reproduction in any medium, provided the original work is properly cited and is not used for commercial purposes.

© 2023 The Authors. *International Journal of Cancer* published by John Wiley & Sons Ltd on behalf of UICC.

KEYWORDS

biomarkers, lipid imaging mass spectrometry, melanoma, molecular histology

What's new?

Here, the authors evaluate the potential of matrix-assisted laser desorption/ionization lipid imaging mass spectrometry (LIMS) together with classification models built using artificial intelligence to classify samples of nevus, melanoma, and metastatic melanoma. They find that, looking at the alterations in the lipid profile of the tissues and having built a library of lipid signatures using LIMS, it is possible to automatically detect the presence of tumor cells and even determine if the sample is a primary tumor or a metastasis. The findings pave the way for the development of fast, accurate, and automatized protocols for the screening of melanoma samples.

1 | INTRODUCTION

Although cutaneous melanomas represent only 5% of all skin cancers, it is the most lethal due to its high rate to metastasis and the lack of effective treatments in advanced stages. In clinical practice, prognosis of melanoma is based on the Breslow index, the presence of ulceration, and sentinel node evaluation.¹ Around 10% of melanoma recurrences within 5 years of follow-up have been described² for early stage lesions (I and II stages according to AJCC 8th edition).³ Furthermore, a recent study showed that in a cohort of 784 melanoma patients, 53.8% of all metastatic patients had an I–II initial stage.⁴ These facts support the view that many early melanomas with a biological ability to metastasize are not identified by classical pathological markers.

Detection of melanoma, even at early stages, is routinely performed in the diagnosis services by pathologists and dermatologists. However, the steady raise in the number of possible cases of melanoma is increasing the pressure in such services. Furthermore, despite the accuracy of a well-trained pathologist, there are still complex cases in which diagnosis is not simple.⁵ Therefore, developing new complementary methodologies that may help with the diagnosis and prognosis is a very active research field. For example, in the last years several optical and proteomic approaches have appeared,^{6,7} aiming at improving diagnosis.

A different approach to the problem of achieving an accurate diagnosis is offered by lipid imaging mass spectrometry (LIMS). This technique enables direct exploration of tissue sections using a mass spectrometer.⁸ The starting point is a fresh frozen sample, which is sectioned using a cryomicrotome (Figure 1). The sections, usually 10–20 μm -thick, are deposited in a microscope glass slide and covered with a matrix that enables the extraction of the molecules with the aid of a laser. Then, a grid of coordinates is defined, which will become the pixels in the final images. The mass spectrometer scans the sample, acquiring a mass spectrum at each coordinate. The result is the distribution map of each of the analytes extracted from the tissue, without the need of a previous labeling.⁹ When the targeted molecules are lipids, the technique becomes a kind of digital molecular histology that enables visualization of each cell type in a given tissue, ultimately in base to their metabolic signature.^{10,11}

Certainly, lipids, which are not genetically encoded, are, directly or indirectly, primarily or secondarily, involved in all main metabolic processes of a cell: from structure to signaling, apoptosis, and so forth.^{12–15} Therefore, each cell in a given metabolic stage presents a

well-defined, tightly regulated, lipid fingerprint.¹⁶ In other words, subtle variations in the metabolic status of a cell involve modifications in lipid expression. For example, we demonstrated in the past that the maturation of the colonocytes as they differentiate along the crypts involves a quantifiable modification of the lipidome.¹⁷ Some of the species exhibit a gradient along the crypt that is maintained among individuals and that is different from the lipid fingerprint of the cells in the lamina propria. Furthermore, the fingerprint of the colonocytes is strongly altered in a sample of neoplastic tissue and therefore, it may serve for early detection of the disease.^{18,19}

We have also demonstrated recently that it is possible to establish at least seven different segments in the nephron according to the lipid fingerprint and that the, in some case subtle, differences in lipid profile between these segments are preserved among individuals.²⁰ Similar observations were also made regarding nevus.²¹ In that case, we demonstrated that epidermis, dermis, and melanocytes present also well-defined fingerprints. Deep analysis of the results from nevi pointed to a difference in the lipid expression between superficial melanocytes and those that have migrated to deeper areas of the dermis. Very likely, such variation is due to the maturation process of the melanocytes.^{22,23}

We exploit here the malignancy state-associated changes in lipid metabolism of melanocytic cells for diagnostic benefit and explore the use of LIMS to classify patient samples into nevus, primary melanoma, and metastasis from melanoma. Previous works already explored the metabolite expression in sections of primary melanoma using mass spectrometry,²⁴ demonstrating that the technique enables extracting the metabolic signature from different cellular populations: melanoma cells, connective tissue, macrophages, and lymphocytes, although the spatial resolution at which images were recorded, 50 μm /pixel, limited somehow precise extraction of such signatures. In a recent work, Lazova et al used mass spectrometry to probe different points across sections and TMA cores of nevus and primary melanoma, concluding that it is possible to build classifiers using the protein fingerprint recovered directly from the tissue.²⁵ Using the same approach, Lazova et al. demonstrated that the technique is also able to identify proliferative nodules within a benign congenital nevus²⁶ and to distinguish between Spitz nevi from Spitzoid malignant melanoma.²⁷ Using DESI in a reduced cohort of samples, Qi et al. identified cholesterol as a possible biomarker in human melanocytic nevi,²⁸ although the conclusions reached in that study need further validation in a larger collection of samples and their technique did not offer

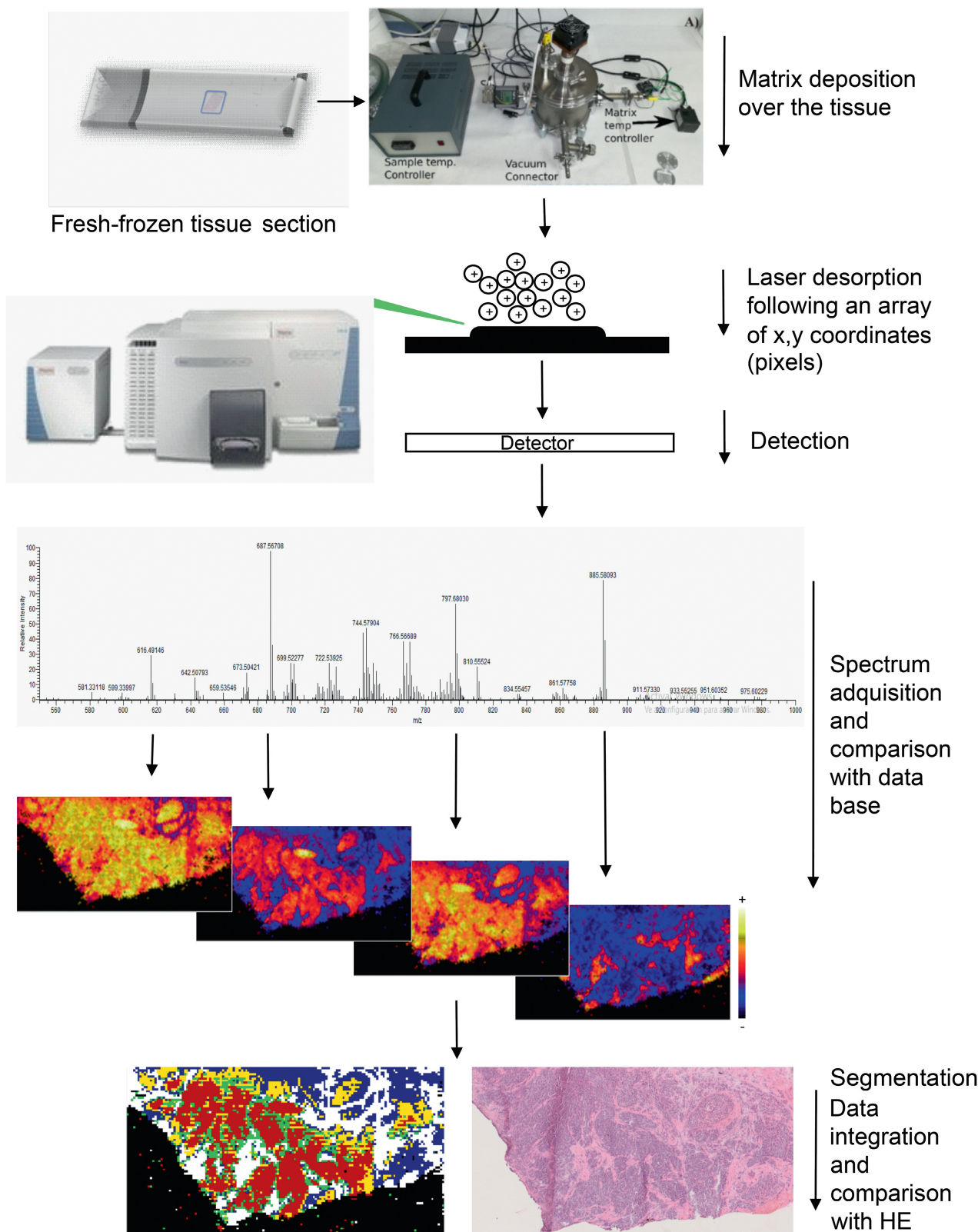


FIGURE 1 Flow diagram of the protocol used in this work in LIMS experiments. Samples are fresh-frozen, trying to avoid the use of OCT or any other substance that may alter the lipid distribution. Then, 16 μm -thick sections are obtained with the aid of a cryomicrotome and are deposited on a plain glass slide. Next, they are covered with 1,5-diaminonaphthalene and introduced in the MALDI source of the mass spectrometer, where they are scanned following a grid of coordinates separated 25 μm . The spectrometer acquires one mass spectrum at each coordinate. The original distribution of the detected species is reconstructed by integrating each m/z and representing its intensity against the coordinates. Finally, a segmentation analysis is performed to determine the lipid fingerprints (= cell populations) in the section.

enough spatial resolution to associate cholesterol changes to cell populations. Other studies using techniques without spatial localization also reported the possibility of using lipid biomarkers for detection of melanoma.²⁹ As it can be seen, none of those previous studies included samples from nevi, primary melanoma, and metastatic melanoma. On the other hand, our own studies in cell cultures point to a differential lipid profile of benign and tumor melanocytic cells, and between the latter, depending on their proliferation potential.³⁰ Demonstrating that LIMS is not only able to classify samples into tumor and non-tumor but also to identify if a sample is a metastasis or a primary tumor is of paramount importance, because it would set the foundations for the development of new and powerful diagnostic techniques.

2 | MATERIALS AND METHODS

Samples and data from patients were collected from 2017 to 2020 and provided by the Pathology Departments of Cruces (Barakaldo, Spain) and Galdakao-Usansolo (Galdakao, Spain) University Hospitals, and by the Department of Dermatology of the Arnau de Vilanova University Hospital (Lleida, Spain). Disease stages were classified according to AJCC, 8th edition.³ Clinical and diagnostic data for each patient were collected retrospectively from centralized electronic and/or paper medical records. A total of 15 nevi, 24 primary melanomas and 14 metastasis were collected, along with the clinical information, including gender, age at the primary tumor, localization of the primary melanoma, localization of metastasis, stage, and histological subtypes (SSM—superficial spreading melanoma, NM—nodular melanoma, ALM—acrolentiginous melanoma, LMM—lentigo maligna melanoma, Table 1).

The age of the patients ranged from 19 to 96 years, with a similar gender distribution. Regarding the histopathological classification, most of the nevus were intradermal ($n = 11$), although a compound nevus and a junctional nevus were also included. The primary melanoma samples corresponded to SSM ($n = 19$), NM ($n = 2$), LMM ($n = 1$), and ALM ($n = 2$). Finally, all metastasis samples were diagnosed as locoregional in transit metastasis.

2.1 | Immunohistochemistry

Biopsies were frozen at -80°C , avoiding the use of OCT or any other compound that could perturb the original lipid distribution. Stepwise sectioning of the frozen tissues was conducted by a conventional cryomicrotome. First, $4\ \mu\text{m}$ -thick sections were collected for hematoxylin-eosin (H&E) staining (Geminis AS Automated Stainer, Eindhoven, Netherland) and for Immunohistochemistry (IHC) of Melan A and HMB45 melanocyte biomarkers. Melan A, also known as MART-1 (melanoma antigen recognized by T cells) marks both melanocytes from nevi and melanoma, while HMB45 specifically marks melanoma cells. IHC was performed using the EnvisionTMG|2 System/AP kit. Optical images were recorded using a NanoZoomer S210 Digital slide scanner (Hamamatsu C13239-01). Melan A (Anti-MelanA

TABLE 1 Clinical information of the patients included in this work.

	Nevus	Melanoma	Metastasis
Number	15	24	14
Age (range)	19–84	32–96	25–91
Gender			
Female	8	11	5
Male	7	13	9
Localization			
Head and neck	2	2	2
Trunk	7	7	4
Upper extremity	1	6	2
Lower extremity	0	5	3
Hand and foot	4	4	1
ND			2
Histology			
Intradermal	11		
Compound	3		
Junctional	1		
LMM		1	1
SSM		19	1
NM		2	3
ALM		2	2
ND			7
Stage (AJCC)			
In situ		1	
I		4	
II		16	
IV		3	

Abbreviations: ALM, acrolentiginous melanoma; LMM, lentigo maligna melanoma; ND, not determined; NM, nodular melanoma; SSM, superficial spreading melanoma.

antibody [EP1422Y]) and MB45 (Anti-Melanoma gp100 antibody [EPR4864]), both from Abcam (Cambridge, CB2 0AX, UK) were used to identify melanoma cells because they recognize the group of proteins gp-100/Pmel-17 specific to melanosomes. Second, sections of $16\ \mu\text{m}$ thickness were obtained for LIMS. The areas to be scanned were selected using the H&E and IHC optical images. One must take into account that the whole area of the sections could not be explored, due the speed of the mass spectrometer (see below), and lipid propensity to oxidation. Finally, the sections explored by LIMS were stained with H&E, so the pathologists could annotate the histological areas and structures in order to correlate them with the segments obtained from the analysis of the LIMS images. In a small number of cases, the post-MALDI H&E could not be used because technical problems (mainly, the tissue folded during staining, because the glass slides did not have any fixation to avoid altering the original lipid distribution). In those cases, the H&E of a consecutive section had to be used, which slightly complicated the annotation of the segmentation images.

2.2 | LIMS experiments

Histological sections from 53 different samples were prepared and analyzed by LIMS as described in Garate et al.²¹ A schematic of the protocol may be found in Figure 1. Briefly, 1,5-diaminonaphthalene (DAN) was used as matrix and deposited with the aid of our in-house designed sublimator.³¹ The sections were scanned in negative polarity, using the orbitrap analyzer of a MALDI-LTQ-Orbitrap XL (Thermo Fisher, San Jose, CA, USA), equipped with a modified MALDI source.³² Previous works have demonstrated that such polarity enables the detection of a larger number of lipid classes, with less interference of adducts formation.³³

Data were acquired with a mass resolution of 60,000 at $m/z = 400$. Two microscans of 10 laser shots were averaged for each pixel using a 25 μm raster size. With these settings, the spectrometer recorded one pixel every 2 s, and therefore, it was necessary to limit the area of the sample to be scanned, to avoid long exposures of the tissue to room temperature conditions. Spectra were processed using in-house developed software, built in Matlab (MathWorks, Natick, USA). Lipid assignment was carried out using the m/z value, the on-tissue MS/MS and MS^3 (whenever the signal intensity permitted it) data and UHPLC/ESI-MS/MS results obtained from the analysis of the extracts from the same samples. With this procedure, in most cases it was not possible to distinguish between ether and vinyl-ether lipids.

Data from each section were analyzed using a segmentation algorithm (HD-RCA)³⁴ to isolate and identify the lipid signatures of each histological area in the section. To establish the number of segments on each image, a heuristic approach was used: the initial number of segments was set to 10 for nevus and melanoma and 5 for metastasis. Then, the segments suggested by the algorithm were verified by examining their correlation: those segments with correlations higher than 95% were grouped together, because such a high correlation seems to indicate that they define similar histologic areas. Each segment was colored using a color scale bar and the correlation between segments. The two segments with the lowest correlation between their lipid signatures were assigned the colors at both ends of the scale and the rest of the segments received colors according to their correlation. Thus, those segments that present colors that are closer in the scale, present more similar lipid fingerprint. Besides, each section presents a unique composition and therefore, similar colors in different sections may correspond to different cell populations. The signatures from the segments obtained from each section were later used in subsequent multi-experiment statistical analysis.

The spectra were filtered before statistical analysis, to avoid introduction of excessive noise. Of the 488 mass channels, only 90 exhibited a SD lower than their mean intensity in the three conditions. Then, the MS/MS and MS^3 (if available) spectra of each species was analyzed to provide a sound assignment. To evaluate the statistical significance of the differences in the lipid fingerprints among nevus melanocytes, primary melanoma and metastasis, Levene test, ANOVA univariate statistical analysis and Tukey/Games Howell post hoc were computed using SPSS Statistics 17.0 (IBM, Armonk, NY,

USA). The Levene test determines the homogeneity of variance ($H_0 =$ groups have equivalent variance) to choose the post hoc method: Tukey if Levene $p \geq .05$ and Games-Howell if Levene $p \leq .05$. PCA analysis and classification models were carried out using Orange Biolab V.2.7.8 (Ljubljana, Slovenia).

3 | RESULTS

3.1 | Identification of melanoma histological structures by LIMS

Understanding the histology of a nevus using the lipid fingerprint provided by a LIMS experiment is relatively simple. Nevus are usually well-organized and structured lesions in which epidermis, dermis, and melanocyte-rich regions are readily identified. This is clearly seen in Figure 2, where the comparison between the H&E image of a nevus, the segmentation of a LIMS experiment and the distribution of three representative lipids is shown.

The nevus section shows slight papillomatous growth, at the expense of melanocytes in the dermis, with growth in more superficial aggregates. Melanocytes in the dermal depth tend to separate or to be more diffusely arranged. A certain fibrosclerosis in the papillary dermis is also observed. The epidermis is thin and an annex to the middle dermis can be identified. The segmentation image is built grouping together pixels with similar lipid fingerprint and assigning each group (segment) a color, using the color bar in the figure. The resulting image highlights the tissue's architecture from a molecular point of view. For example, clear difference between the epidermis (white segment) and the rest of the tissue is readily seen. The melanocytes and the surrounding stroma exhibit a high degree of heterogeneity, highlighted by their division in several segments that follow the melanocytic aggregates (light blue, yellow, and orange) and the surrounding stroma (black and dark blue). Ultimately, the segmentation images reflect the differential spatial distribution of the lipid species detected. As an example, the distribution of three representative species is shown in the figure. Sphingomyelin (SM) 34:1 presents a higher abundance in the stroma of nevus, while is slightly less abundant in melanocytes. Conversely, phosphatidylethanolamine (PE) 36:2 follows the opposite trend, being more abundant in the epidermis of nevus. The concentration of phosphatidylinositol (PI) 38:3 is also more abundant in the stroma, but with a different distribution, pointing to changes in expression between cell populations. Actually, the segmentation image in Figure 2 is a sort of summary of these lipid distributions: each cell population presents a well-defined lipid profile. Consequently, when the pixels in the LIMS image are grouped based on their lipidome, as in the segmentation image, the whole tissue architecture emerges. In some sense, LIMS is a kind of molecular histology.

Figure 2 (and Figure S1 of the supplemental material) also show examples of melanoma and metastasis sections. The primary tumor presents an epidermal component that affects the hair follicle at a level deeper than the infundibular portion. The most eye-catching

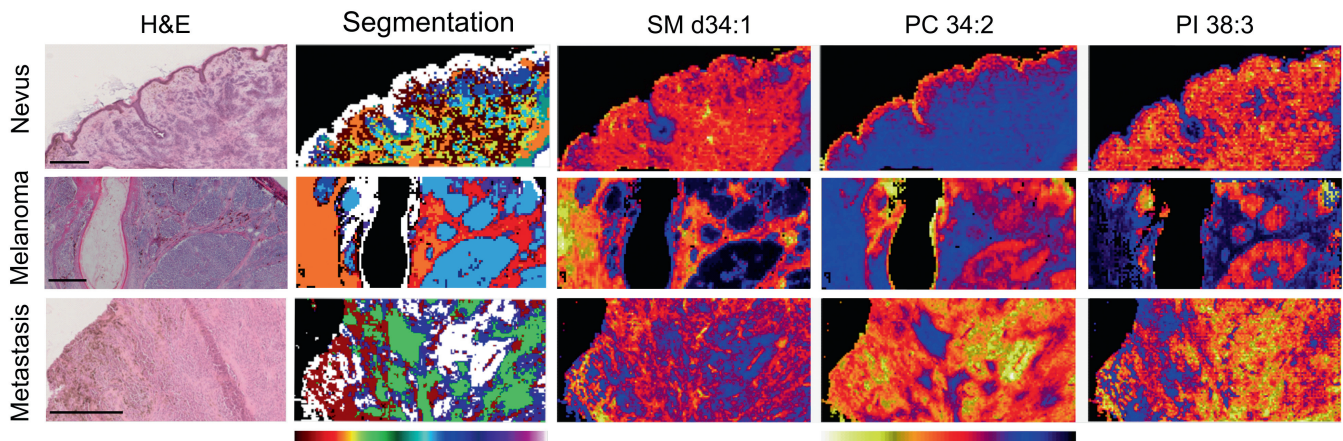


FIGURE 2 Lipid fingerprint highlights the histology of the tissue. H&E optical images, segmentation and distribution images of SM 34:1, PE 36:2 and PI 38:3 over sections of nevus, melanoma and metastasis from melanoma. The LIMS experiment was recorded in negative polarity at 25 $\mu\text{m}/\text{pixel}$ of spatial resolution and the segments were colored using the color bar shown in the figure and the degree of correlation between segments: the proximity of the colors in the scale indicates the correlation between the lipid fingerprint of the segments. Relative abundance of the lipids follows a black-blue-red-yellow-white scale. Scale bar = 1 mm.

feature of the image is the hair follicle with cystic dilation in addition to keratin and brown pigment. The follicular epithelium is hyperplastic and occupied by a disorderly growth of individual melanocytes, forming thecae. The tumoral part that affects the dermis shows large aggregates, with a diffuse growth of epithelioid melanocytes with some pigment, melanophages, and occasionally intratumoral lymphocytes. The LIMS image faithfully follows the histology in the H&E image. On the left side of the segmentation image, the dilated hair follicle appears in black, while its luminal keratin and even the keratin of the stratum corneum appear as a white segment. Tumor melanocytes are predominantly in the blue segment, both in dermal aggregates and in the epidermis. Moreover, a peritumoral region can be identified of tumor melanocytes and stromal tissue with different lipid profile. The stroma is coincident with the red and orange segments. In this latter segment, lymphocytes and melanophages appear as spots. When further segments are created (not shown), the immune cells become more evident. In addition, perifollicular collagen regions can also be detected.

The example of metastasis in Figure 2, is a collagenous-rich stroma infiltrated by a tumor with scattered and heterogeneous presence of pigment. Tumor cells are distributed almost continuously, sometimes forming vertical trails. Collagen and other elements of the stroma, such as blood vessels, can be seen between these trails. In the segmentation image, the melanocytes appear as green and brown patches and the stroma in blue and white. Correspondence between histological and segmentation images is not straightforward because the H&E corresponds to a consecutive section and the differences between histological regions is more evident in the segmentation image. The striking contrast between the colors of the segments increases the visibility of the small color differences in the H&E image.

A look at the distribution of the three lipid species shown as example in Figure 2, highlights once more that the segmentation

analysis is a reflection of the differences in lipid profile among the cells composing the tissue. SM 34:1 presents a strong difference in relative abundance between stroma and tumor cells in the melanoma section, while it presents lower concentration in metastatic cells. PE 36:2 is more abundant in tumor cells in the melanoma section and is maximized in metastatic tumor cells. Meanwhile, PI 38:3 also shows a different trend: its relative abundance strongly increases in the tumor nodules in melanoma and shows a relatively higher abundance in the stroma of metastasis and in the tumor cells that correlate with the green segment, highlighting the existence of different tumor cell populations.

The inherent complexity of the tumoral tissues complicates to a great extent the process of building a classifier, as a single sample very often presents different tumor cell populations with (sometimes slightly) different lipid signatures. As a first approximation, we extracted from each section all those signatures that can be associated to tumor cells and included them in the classifiers, leaving aside those lipid fingerprints corresponding to other areas (fibroblasts, sclerotic tissue, necrotic areas, etc.). Extraction of lipid signatures was also guided by the comparison with the Melan A staining experiments. Figure 3 shows the comparison between example images of H&E staining, Melan A and the segmentation of a LIMS experiment carried out over samples of intradermic nevus, primary melanoma and metastasis.

In the segmentation image of the nevus, the three main histological regions are clearly visible: epidermis in white, dermis in yellow and the melanocyte-rich regions in red and brown. Conversely, melanomas are, in general, highly heterogeneous, presenting a variable number of regions in each sample. Figure 3, middle row, shows a histological section of a superficial spreading primary melanoma in stage IIB.³ The lesion exhibits an asymmetric growth and a zone of dermal invasion with large nodules, separated by connective tissue and some

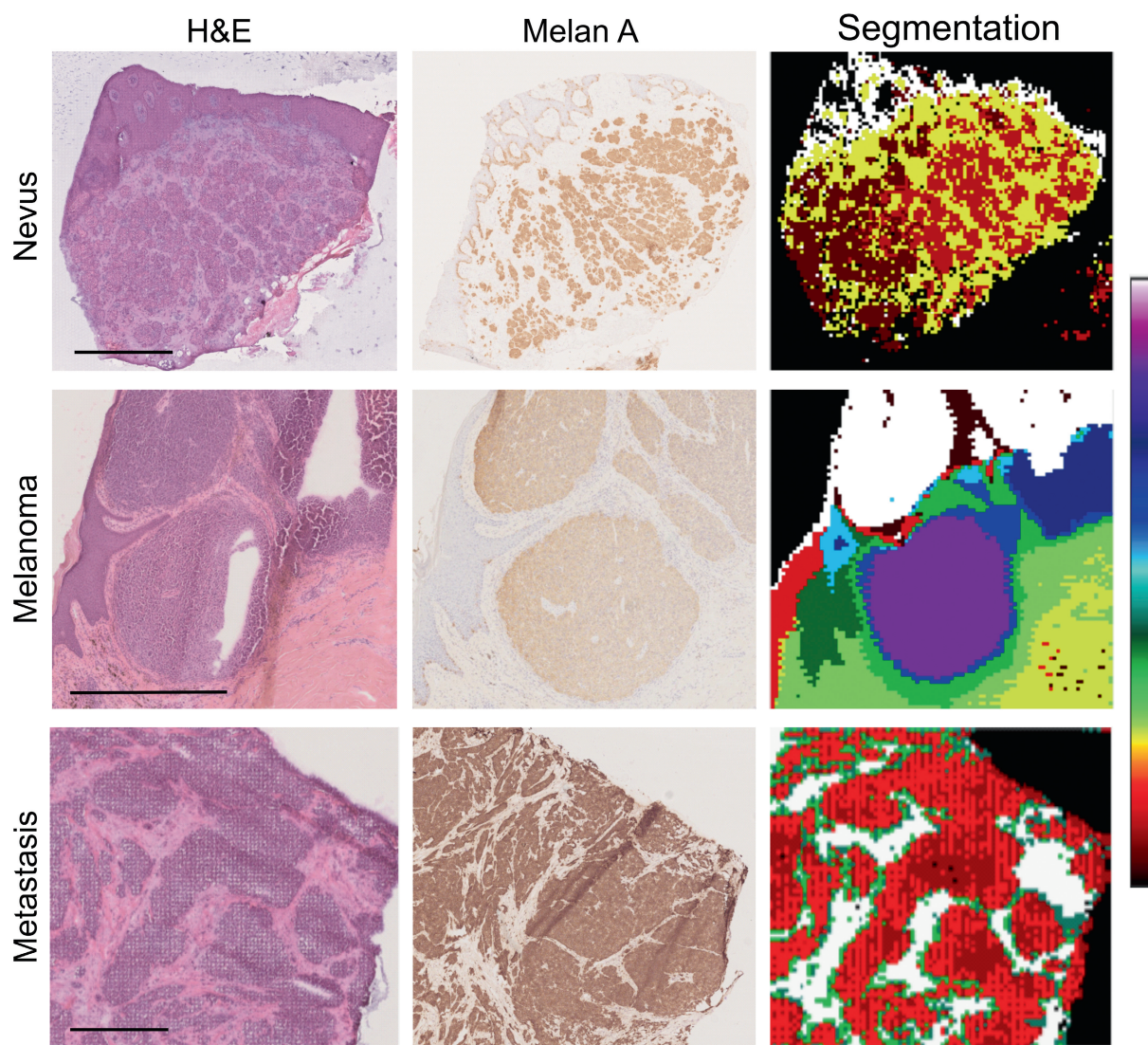


FIGURE 3 Segmentation images describe the histology of the tissue. Comparison between the images of H&E staining, Melan A biomarker distribution assessed by IHC and the segmentation analysis of LIMS carried out over the same histological sections. Top row: a nevus section; middle: primary melanoma and bottom row: metastasis from melanoma. LIMS experiment recorded in negative polarity at a pixel size of 25 μm . The algorithm automatically detected histological areas based on the lipid composition and assigned colors according to the color bar shown in the figure, and the correlation between lipid fingerprints. Scale bar = 1 mm.

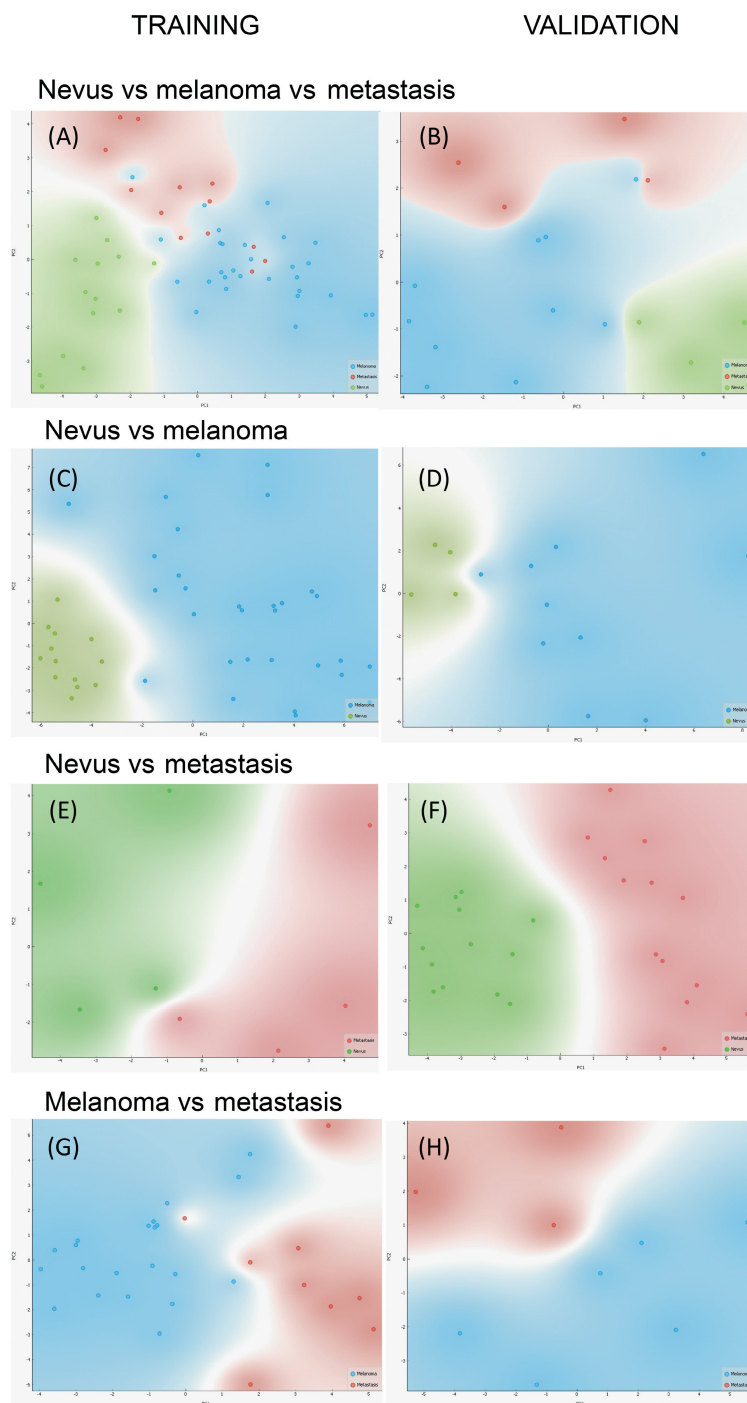
lymphocytes and melanophages. Tumor nests are clearly defined and represented in the LIMS segmentation image as violet and white segments, indicating that at least two different tumor cell populations exist. Moreover, the lymphocytes surrounding the melanocyte nodules appear as a blue segment. The epidermis matches the red segment, while other cells such as fibroblasts and stroma in general appear in green.

Interestingly, heterogeneity is lower in most of the analyzed metastasis. For example, the metastasis section in Figure 3, bottom row, clearly shows three regions: tumor nodes (bright and dark red), a border segment that delimits the tumor nodes that is not evident in the optical image (green segment) and collagen-rich tissue (white segment).

3.2 | Differential lipid fingerprint of melanocytic cells from nevus, primary melanoma and metastasis

Figure 4 shows the scores plot of the principal component analysis (PCA) of the lipid signatures extracted from the samples using LIMS. Melanocytic lipid signatures come from nevus sections, while more than one lipid fingerprint was extracted from each primary and metastatic melanoma sample. Within each condition, the samples were randomly divided into training and validation sets and multiple comparisons were carried out. When the three conditions were included in the analysis, Figure 4A,B, a good separation of melanocytic samples from those of tumor cells was observed in the training set, while incomplete separation was observed between melanoma and

FIGURE 4 Scores plots of principal components analysis (PCA) of the lipid fingerprints. The samples were randomly divided into training and validation sets (2/3 and 1/3 of the samples, respectively) before being subjected to several PCA: (A and B) joint analysis of all samples; (C and D) analysis of nevus and primary melanoma lipidomes; (E and F) nevus versus metastasis and (G and H) metastasis versus primary melanoma. In all cases, a classifier built using logistic regression and the discriminant lipids selected in the training set, was able to achieve a perfect classification of the validation group samples (Table S1 of the supplemental material).



metastasis. However, the analysis of the samples in the validation set using only those lipid species that showed statistically significant differences in the training set (potential biomarkers), resulted in a perfect separation of the three types of samples (Figure 4B). Three classification models were tested using the potential lipid biomarkers: support vector machine (SVM), Naïve Bayes and Logistic Regression, achieving with the latter a perfect classification of the samples (see Table S1).

Next, the lipid fingerprints of nevus melanocytes were compared with those of primary melanoma and metastasis (Figure 4C–F). A

perfect separation was achieved all cases, highlighting the strong metabolic changes that accompany tumor transformation. The classification models also exhibited outstanding performances, both in the training and validation sets, with logistic regression achieving perfect separation.

Classification of primary and metastatic samples was not perfect in the training set (Figure 4G,H), with only two of the metastasis misclassified as primary tumors. However, sample classification was perfect in the validation group, using the potential lipid biomarkers (Table S1).

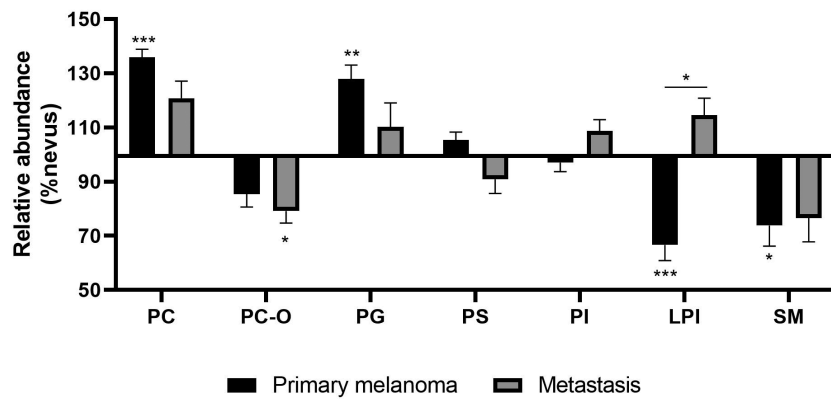


FIGURE 5 Significant changes in lipid fingerprint between conditions. Values are expressed as the relative abundance of the corresponding lipid group, 100% being the abundance in nevus melanocytes. PC and PE are presented together as “PC” due to the (presumably) large number of isobaric species contributing to each mass channel. Likewise, PC-O/P and PE-O/P are presented as PC-O. * $p < .05$; ** $p < .01$; *** $p < .001$ versus nevus.

4 | DISCUSSION

The results presented herein clearly demonstrate that a substantial change in the lipid fingerprint accompanies tumor transformation. Such changes enable building classification models with performances between 90% and 100% (depending on the algorithm) when biopsies from nevus, primary melanoma and metastatic melanoma are included and with perfect performance in binary comparisons. A consequence of this observation is that LIMS can be used in conjunction with such classifiers to identify tumor cells directly from tissue sections, opening the door to the use of this technique in clinics for fast and automated sample screening.

Comparison of the relative abundance of the main lipid classes recorded by LIMS may be found in Figure 5, while the potential biomarkers are collected in Figure S2. There are statistically significant variations in lysophosphatidylinositol (LPI), phosphatidylcholine/phosphatidylethanolamine (PC/PE), PC/PE ether/plasmalogens (O/P), phosphatidylglycerol (PG) and SM classes. PC and PE were grouped together in a single graphics, due to the existence of isobaric species contributing to each peak in the mass spectrum. Similarly, PC/PE O/P were also grouped in a single class. Apparently, there is an increase of PC/PE in primary melanoma, which is partly reverted in metastasis. Interestingly, the changes in PC/PE O/P follow an opposite trend to those of the di-acyl PC/PE species. Also significant is the decrease in LPI detected in primary melanoma. Finally, there is an increase in PG and a decrease in SM from nevus to melanoma that are again partially reverted in metastasis.

Detailed analysis of the relative abundance of the individual species may be found in Figure S2 and Table S2. A close look at the PI class—significantly involved in signaling—shows a decrease in the relative abundance of arachidonic acid (AA, 20:4)-containing species, and an increase in the species with mono- and di-unsaturated fatty acids (MUFA and DUFA) from nevi to primary melanoma. For some of the species, this trend is reverted in metastasis, which exhibits expression levels closer to those of nevus. This kind of trans-acylation process would explain the absence of changes in the relative abundance of total PI between the three conditions and it was also observed in other systems.¹⁸

A reduced number of LPI and LPI-O/P species presented changes between samples. The most remarkable variation is the decrease in the relative abundance of LPI 20:4, which mimics those observed in AA-containing PI species. It is tempting to speculate that this results from a higher demand of AA for provision of inflammation-related eicosanoid mediators.

A limited number of PG and PS species were also detected, but in both cases, there is an increase in the relative abundance of MUFA/DUFA-containing species and a decrease in PUFA in primary melanoma. Such trend is reversed in metastasis, showing a more similar composition to that found in melanocytes.

The analysis in Figure 4 may be regarded as a simplified approach. Certainly, there is still a wealth of information present in the LIMS data that was not exploited in the present work, such as the presence of infiltrating cells, areas with necrosis, cell density or the presence of different clones of tumor cells. Although interpretation is not simple, creation of a library of lipid fingerprints to automatically annotate the tissue sections may yield invaluable information for the diagnosis and prognosis of the disease. Construction of such library would require of detailed analysis of hundreds of samples and careful comparison with the LIMS images. Figures S3–S5 constitute a gradient in complexity and illustrate how LIMS is able to highlight the heterogeneity of tumor samples. The Melan A image of a primary melanoma in Figure S3 shows very homogenous tumor cells, in brown, forming nests, surrounded by lymphocytes and some eosinophils in blue. Such organization is clearly captured by the segmentation image of the corresponding LIMS experiment, in which the tumor cells are grouped in the red segment, while the inflammatory cellularity appears in blue and the dermis in white. Interestingly, all tumor cells show a similar lipidome. Actually, increasing the number of segments of the image did not divide the tumor nodules in different groups, demonstrating that they truly present non-differentiable lipidomes. The observations in Figure S3 contrast with the findings shown in Figure S4 from a different primary melanoma. In this second example, the lymphocytes are grouped forming a lymphoid follicle surrounded by tumor and appear in the same segment as the sub-epidermal lymphocytes intermixed with the epidermis. Here, the tumor melanocytes are grouped in three different segments: red, white and brown. Further inspection

of the H&E sample revealed that the tumor cells grouped in the red segment present an important amount of melanin in the cytoplasm, compared to the cells in the other two segments. It would be interesting to use orthogonal techniques to determine if the lipidome of one of the three segments corresponds with a stronger proliferative potential.

The sample in Figure S5 corresponds to a metastasis and constitutes a case in which an extraordinary heterogeneity may be appreciate. A subcutaneous nodule dominates the image, with walls with intense fibrosis. Several solid tumor nodules are clearly seen, with slightly pleomorphic cells of middle size (Figure S5C), with epithelioid and plasmacytoid aspect. Nuclei are mainly hyperchromatic and some present cytoplasmic folding; the cells' cytoplasm are eosinophil and contain a variable amount of pigment. This can also be seen in the septa, where some lymphocytes and macrophages can be identified, together with other stromal cells. The segmentation image shows a variety of lipid signatures (segments), some of them difficult to identify, unless both the optical and segmentation images are superimposed. Tumoral cells appear divided into several segments: from white to blue. But also the stromal cells appear divided in several segments: red, green yellow and orange. In addition, a large fibrotic area correlates with the dark brown segment and there is also a green segment that correlates with a portion of the tissue that was lost during H&E staining. Thus, this sample not only presents heterogeneous tumor cell populations, but also the stromal cells that compose the microenvironment in which the tumor is immersed, show a collection of lipid signatures. Understanding why some tumors present a larger heterogeneity than others and the source of this variation may be the key for the development of new and more precise methodologies for tumor prognosis.

5 | CONCLUSIONS

We present here the LIMS analysis of 53 samples of nevus, primary melanoma and metastatic melanoma. The spatial resolution of the technique allowed us to extract the lipid signature of the melanocytic cells and isolate them from those of other cell populations in the biopsies. Using such lipid fingerprints, it was possible to set up statistical models able to classify the samples attending to their nature: nevus, primary melanoma and metastasis from melanoma. Detailed analysis of the histology of the samples and comparison with the LIMS segmentation images demonstrate that the latter captured key aspects of the samples, such as degree of heterogeneity, the existence of different tumor populations or different tumor microenvironments. Full understanding of the information in the segmentation images is a cumbersome task, as it requires of manual analysis of hundreds of samples by well-trained pathologists and comparison with the segmentation images, but it may enable the design of new automated methodologies for the early and accurate diagnosis of melanoma.

AUTHOR CONTRIBUTIONS

The work reported in the paper has been performed by the authors, unless clearly specified in the text. CHB: data collection, data analysis

and interpretation, generation of figures; Verónica Velasco, Jone Garate and Roberto Fernández: data collection and analysis; Javier Martín-Allende: software generation for data visualization and analysis; Ignacio Zabalza, Juan L. Artola and Rosa M. Martí: sample collection, patient selection; Aintzane Asumendi, Egoitz Astigarraga and Gabriel Barreda-Gómez: management, rising resources; Olatz Fresnedo and Begoña Ochoa: data analysis and interpretation, draft generation; María D. Boyano and José A. Fernández: management, rising resources, conceived experiments and analyzed data, generation of first draft. All authors were involved in writing the paper and had final approval of the submitted and published version.

ACKNOWLEDGEMENTS

The authors acknowledge the technical support and mass spectrometry resources to SGIker (UPV/EHU). Moreover, the authors are grateful to the Basque Biobank for providing the biopsy samples and in particular, to Anna Crespo for their technical support with the cryosectioning of tissues.

FUNDING INFORMATION

This project was supported by grants from the Basque Government (KK2017-041 and KK2020-00069 to JAF, BO and MDB and grant IT1491-22 to JAF), the UPV/EHU (GIU17/066 to MDB) and by MINECO (RTC-2015-3693-1).

CONFLICT OF INTEREST STATEMENT

The authors declare no conflicts of interest.

DATA AVAILABILITY STATEMENT

The datasets used and analyzed during the current study are available here: <http://doi.org/10.5281/zenodo.10036138>, together with all the original H&E, HMB 45, Melan A, and segmentation images. Very high-resolution histological images in .ndpi format and other data that support the findings of this study are available from the corresponding author upon request. The algorithm used for the conversion of the images from mzml into imzml can be found here: <https://github.com/imzML/imzML/blob/master/imagingMS.obo>

ETHICS STATEMENT


The study was conducted in accordance with the Declaration of Helsinki principles and it was approved by the Euskadi (reference PI2017035) and Lleida (reference 011-17) Ethics Committees. Written informed consents were obtained from all participants.

ORCID

Cristina Huergo-Baños  <https://orcid.org/0000-0001-9799-9276>

Verónica Velasco  <https://orcid.org/0000-0003-3759-2639>

Jone Garate  <https://orcid.org/0000-0003-2258-7116>

Javier Martín-Allende  <https://orcid.org/0000-0001-9186-9075>

Rosa M. Martí  <https://orcid.org/0000-0001-6866-6114>

Aintzane Asumendi  <https://orcid.org/0000-0002-2156-2323>

Egoitz Astigarraga  <https://orcid.org/0000-0002-0338-5554>

Gabriel Barreda-Gómez  <https://orcid.org/0000-0002-8330-1567>

Olatz Fresnedo  <https://orcid.org/0000-0002-1172-1423>

Begoña Ochoa  <https://orcid.org/0000-0002-1580-7160>

Maria D. Boyano  <https://orcid.org/0000-0001-6051-1054>

José A. Fernández  <https://orcid.org/0000-0002-7315-2326>

REFERENCES

1. Michielin O, van Akkooi ACJ, Ascierto PA, et al. Cutaneous melanoma: ESMO clinical practice guidelines for diagnosis, treatment and follow-up—Approved by the ESMO guidelines committee: February 2002, last update September 2019. *Ann Oncol*. 2019;30(12):1884-1901.
2. Bajaj S, Donnelly D, Call M, et al. Melanoma prognosis: accuracy of the American Joint Committee on Cancer Staging Manual Eighth Edition. *J Natl Cancer Inst*. 2020;112(9):921-928.
3. Gershenwald JE, Scolyer RA. Melanoma staging: American Joint Committee on Cancer (AJCC) 8th edition and beyond. *Ann Surg Oncol*. 2018;25(8):2105-2110.
4. Ertekin SS, Podlipnik S, Riquelme-Mc Loughlin C, et al. Initial stage of cutaneous primary melanoma plays a key role in the pattern and timing of disease recurrence. *Acta Derm Venereol*. 2021;101(7):adv00502-3832.
5. Magro CM, Crowson AN, Mihm MC. Unusual variants of malignant melanoma. *Mod Pathol*. 2006;19(2):S41-S70.
6. Polesie S, Gillstedt M, Kittler H, Rinner C, Tschandl P, Paoli J. Assessment of melanoma thickness based on dermoscopy images: an open, web-based, international, diagnostic study. *J Eur Acad Dermatol Venereol*. 2022;36(11):2002-2007.
7. Casadonte R, Kriegsmann M, Kriegsmann K, et al. Imaging mass spectrometry-based proteomic analysis to differentiate melanocytic nevi and malignant melanoma. *Cancers (Basel)*. 2021;13(13):3197. doi: [10.3390/cancers13133197](https://doi.org/10.3390/cancers13133197)
8. Caprioli RM, Farmer TB, Zhang HY, et al. Molecular imaging of biological samples by MALDI MS. Abstracts of Papers of the American Chemical Society. 1997; 214: 113-ANYL.
9. Baker TC, Han J, Borchers CH. Recent advancements in matrix-assisted laser desorption/ionization mass spectrometry imaging. *Curr Opin Biotechnol*. 2017;43:62-69.
10. Comi TJ, Do TD, Rubakhin SS, et al. Categorizing cells on the basis of their chemical profiles: Progress in single-cell mass spectrometry. *J Am Chem Soc*. 2017;139(11):3920-3929.
11. Gilmore IS, Heiles S, Pieterse CL. Metabolic imaging at the single-cell scale: recent advances in mass spectrometry imaging. *Annu Rev Anal Chem*. 2019;12(1):201-224.
12. Gross RW. The evolution of lipidomics through space and time. *Biochim Biophys Acta Mol Cell Biol Lipids*. 2017;1862(8):731-739.
13. Sethi S, Brietzke E. Recent advances in lipidomics: analytical and clinical perspectives. *Prostaglandins Other Lipid Mediat*. 2017;128-129: 8-16.
14. Han X. Lipidomics for studying metabolism. *Nat Rev Endocrinol*. 2016; 12:668-679.
15. Kimura T, Jennings W, Epanand RM. Roles of specific lipid species in the cell and their molecular mechanism. *Prog Lipid Res*. 2016;62: 75-92.
16. Tajik M, Baharfar M, Donald WA. Single-cell mass spectrometry. *Trends Biotechnol*. 2022;40(11):1374-1392.
17. Garate J, Fernandez R, Lage S, et al. Imaging mass spectrometry increased resolution using 2-mercaptobenzothiazole and 2,5-diaminonaphthalene matrices: application to lipid distribution in human colon. *Anal Bioanal Chem*. 2015;407:4697-4708.
18. Bestard-Escalas J, Garate J, Maimó-Barceló A, et al. Lipid fingerprint image accurately conveys human colon cell pathophysiologic state: a solid candidate as biomarker. *Biochim Biophys Acta Mol Cell Biol Lipids*. 2016;1861(12, Part A):1942-1950.
19. Lopez DH, Bestard-Escalas J, Garate J, et al. Tissue-selective alteration of ethanalamine plasmalogen metabolism in dedifferentiated colon mucosa. *Biochim Biophys Acta Mol Cell Biol Lipids*. 2018;1863(8): 928-938.
20. Martín-Saiz L, Mosteiro L, Solano-Iturri J, et al. High-resolution human kidney molecular histology by imaging mass spectrometry of lipids. *Anal Chem*. 2021;93(27):9364-9372.
21. Garate J, Lage S, Fernández R, et al. Imaging mass spectrometry-based lipidomic approach to classification of architectural features in nevi. *J Invest Dermatol*. 2019;139(9):2055-2058.e7.
22. Bertrand JU, Steingrimsson E, Jouenne F, Paillerets B, Larue L. Melanoma risk and melanocyte biology. *Acta Derm Venereol*. 2020; 100(11):adv00139-3494.
23. Vidács DL, Veréb Z, Bozó R, et al. Phenotypic plasticity of melanocytes derived from human adult skin. *Pigment Cell Melanoma Res*. 2022;35(1):38-51.
24. Sugihara Y, Rivas D, Malm J, et al. Endogenous expression mapping of malignant melanoma by mass spectrometry imaging. *Clin Trans Med*. 2018;7(1):e22.
25. Lazova R, Smoot K, Anderson H, et al. Histopathology-guided mass spectrometry differentiates benign nevi from malignant melanoma. *J Cutan Pathol*. 2020;47(3):226-240.
26. Lazova R, Yang Z, El Habr C, et al. Mass spectrometry imaging can distinguish on a proteomic level between proliferative nodules within a benign congenital nevus and malignant melanoma. *Am J Dermatopathol*. 2017; 39(9):689-695.
27. Lazova R, Seeley EH, Keenan M, Gueorguieva R, Caprioli RM. Imaging mass spectrometry—a new and promising method to differentiate spitz nevi from spitzoid malignant melanomas. *Am J Dermatopathol*. 2012;34(1):82-90.
28. Qi K, Lv Y, Ren Y, et al. Cholesterol was identified as a biomarker in human melanocytic nevi using DESI and DESI/PI mass spectrometry imaging. *Talanta*. 2021;231:122380.
29. Kim H, Lee H, Kim S, et al. Discovery of potential biomarkers in human melanoma cells with different metastatic potential by metabolic and lipidomic profiling. *Sci Rep*. 2017;7(1):8864.
30. Perez-Valle A, Abad-García B, Fresnedo O, et al. A UHPLC-mass spectrometry view of human melanocytic cells uncovers potential lipid biomarkers of melanoma. *Int J Mol Sci*. 2021;22(21):12061.
31. Fernández R, Garate J, Martín-Saiz L, Galetich I, Fernández JA. Matrix sublimation device for MALDI mass spectrometry imaging. *Anal Chem*. 2019;91(1):803-807.
32. Montero R, Abad-García B, Garate J, Martín-Saiz L, Barceló-Coblijn G, Fernández JA. Improving spatial resolution of a LTQ Orbitrap MALDI source. *J Am Soc Mass Spectrom*. 2020;31(8):1755-1758.
33. Garate J, Lage S, Martín-Saiz L, et al. Influence of lipid fragmentation in the data analysis of imaging mass spectrometry experiments. *J Am Soc Mass Spectrom*. 2020;31(3):517-526.
34. Fernández R, Garate J, Tolentino-Cortez T, et al. Microarray and mass spectrometry-based methodology for lipid profiling of tissues and cell cultures. *Anal Chem*. 2019;91(24):15967-15973.

SUPPORTING INFORMATION

Additional supporting information can be found online in the Supporting Information section at the end of this article.

How to cite this article: Huergo-Baños C, Velasco V, Garate J, et al. Lipid fingerprint-based histology accurately classifies nevus, primary melanoma, and metastatic melanoma samples. *Int J Cancer*. 2024;154(4):712-722. doi:[10.1002/ijc.34800](https://doi.org/10.1002/ijc.34800)